J Appl Electrochem (2009) 39:671–679
DOI 10.1007/s10800-008-9707-z

ORIGINAL PAPER

Improved electrochemical properties of $Li(Ni_{0.7}Co_{0.3})O_2$ cathode for lithium ion batteries with controlled sintering conditions

Dae Geun Lee · Ravindra K. Gupta · Yong Soo Cho · Kwang Taek Hwang

Received: 7 May 2008 / Accepted: 24 October 2008 / Published online: 13 November 2008
© Springer Science+Business Media B.V. 2008

Abstract Improved electrochemical properties of $Li(Ni_{0.7}Co_{0.3})O_2$ cathode material are reported. Samples were synthesized by the co-precipitation method with various sintering conditions, namely temperature, time and atmosphere. $Li(Ni_{0.7}Co_{0.3})O_2$ sintered at 850 °C for 14 h in air exhibited the lowest unit cell volume accompanied with relatively higher values of c/a and I_{103}/I_{104} reflection peaks ratios. This also exhibited superior electrochemical properties, such as high charge–discharge capacity, high Coulombic efficiency, and low irreversible capacity loss. This can be attributed to improved hexagonal ordering, crystallinity and morphology. The electrochemical cell parameters were better than the reported ones, probably due to controlled sintering conditions.

Keywords Lithium nickel cobalt oxide · Lithium batteries · Structural properties · Electrochemical properties · Sintering conditions

1 Introduction

Lithium-ion batteries are an attractive power source for a wide variety of applications, namely laptops, cellular phones, digital cameras, and electric or hybrid vehicles [1–5]. Lithium cobalt oxide ($LiCoO_2$) is commercially applied as a cathode active material in lithium-ion batteries due to its easy preparation, good reversibility and high theoretical specific capacity. However, it has some disadvantages, such as a low effective specific capacity, and high toxicity and cost. It also has safety problems, especially when the lithium content (x) is lower than 0.5 in Li_xCoO_2 or charge voltage exceeds 4.3 V [1–6]. Lithium nickel oxide ($LiNiO_2$) has also been proposed as a cathode active material because of its layered structure similar to $LiCoO_2$, high discharge capacity, low cost and the fact that it is environmentally benign. However, synthesis of stoichiometric $LiNiO_2$ on a large scale with an ideal layered structure by the conventional solid state reaction method is difficult. It exhibits poor thermal stability in its highly oxidized state (Ni^{3+}/Ni^{4+}) [3–9]. It also exhibits poor cycling performance due to its structural instability upon cycling [3–6].

Partial doping of Co with 0.2–0.3 mole fraction in Ni-site has been considered as a convenient way to overcome the drawbacks of $LiNiO_2$ as cobalt stabilizes the layered structure in a two dimensional fashion. This improves the reversibility of the intercalation and the deintercalation [3–6, 10–12]. An enhancement in hexagonal ordering of layers improves the electrochemical properties [3–6]. The ordering of Li-sites also improves the electrochemical properties [3, 6, 11]. The electrochemical properties of the electrode material are also sensitive to the microstructure, which strongly depends on the synthesis conditions [4–6, 12–19]. For example, sintering temperature and time are reported to largely affect the structure of $LiNi_{0.8}Co_{0.2}O_2$ and hence the electrochemical properties [15–19].

To the best of our knowledge, no similar study, i.e., effects of sintering temperature, time and atmosphere on structure, microstructure and electrochemical properties,

D. G. Lee · K. T. Hwang
Korea Institute of Ceramic Engineering and Technology, Seoul, Gyeonggi-do 467-843, South Korea

D. G. Lee · R. K. Gupta · Y. S. Cho (✉)
Department of Materials Science and Engineering, Yonsei University, Seoul 120-749, South Korea
e-mail: ycho@yonsei.ac.kr

has been performed on $Li(Ni_{0.7}Co_{0.3})O_2$, though 0.3 mole of Co substitution was noted the best to get a pure two dimensional structure [10, 12]. $Li(Ni_{0.7}Co_3)O_2$ exhibits a layered structure of Li (3a: 0, 0, 0), Ni/Co (3b: 0, 0, 0.5) and O (6c: 0, 0, ~0.24) due to the absence of cation-mixing i.e. Ni and Li in the 3a- and 3b-sites, respectively [10, 12]. The 3a, 3b and 6c are the Wyckoff atomic positions.

In this work effects of sintering conditions, namely temperature, time and atmosphere on structure, morphology and electrochemical properties of $Li(Ni_{0.7}Co_{0.3})O_2$ cathode active material are investigated for understanding the relation between them and improving the electrochemical properties. $Li(Ni_{0.7}Co_{0.3})O_2$ is abbreviated hereafter as LNC. It is also accompanied by the subscripts, T, H and A for sintering temperature, time and atmosphere, respectively.

2 Experimental

LNC was prepared by the co-precipitation method using commercially available Aldrich chemicals, Li_2CO_3 (98.5%), $NiSO_4 \cdot 6H_2O$ (99%) and $CoSO_4 \cdot 6H_2O$ (99.5%). Aqueous solutions of Ni- and Co-salts (1 M both) were mixed together in the 0.7:0.3 molar ratio along with NH_4OH and stirred at ~60 °C for 24 h. The pH of solution was kept ~11.8 using NaOH. The precipitates were filtered and washed, and then mixed with Li_2CO_3 thoroughly using an agate pestle and mortar. An excess Li content, ~1.08 mole, was used to saturate the available Li-sites for inhibiting the occupation of Ni^{2+} ions to the Li-sites [3, 9, 11]. It also compensates the Li loss by volatilization. The sintering conditions for obtaining the LNC powder with a grain size of ~20 μm are shown in Table 1.

The XRD patterns of the samples were collected for the 2θ range of 5–80° in a step of 0.04° using a Rigaku X-ray diffractometer (XRD, D/max-2500/PC, Japan) with CuK_α radiation. The XRD patterns were then refined using a Rietveld analysis program, MAUD, for determining lattice parameters and weight fraction. Crystallite size (D) of powder was calculated at 2θ–18.7° (the strongest peak in the XRD pattern) using the Scherrer formula, $D = 0.94\lambda/\beta\cos(\theta)$, where λ is the wavelength of the X-ray source (1.54056 Å) and β is the full width at half maxima. The Brunauer-Emmett-Teller (BET) surface area was measured using a specific surface area/pore size distribution analyzer (model Belsorp mini, Bel Japan Inc., Japan). A JEOL scanning electron microscope (model JSM-6707F, Japan) was used for microstructural study.

The electrochemical study was performed on CR type 2032 cells constructed using following components in an argon-filled glove box. The positive electrode was prepared using LNC (85 wt.%) as a cathode active material, poly vinylidene fluoride (PVDF, 5 wt.%) as a binder, carbon black (Super-P, 10 wt.%) as an electronic conductor and *n*-methyl-2-pyrrolidone (NMP) as a solvent. The mixture was dried at 120 °C for 12 h in order to evaporate water and then roll-pressed to get the positive electrode of thickness ~60 μm. Lithium metal was used as a counter electrode, Celgard 2500 as a separator and 1 M $LiPF_6$ in ethylene carbonate–ethyl methyl carbonate (1:2 by volume) as an electrolyte. A XENO battery cycler (WBC-3000, Korea) was used for the electrochemical measurement at between 2.8 and 4.5 V at room temperature.

Table 1 Sintering conditions and lattice constants (a and c) for LNC

Sample	Sintering conditions			a (Å)	c (Å)	ϕ (%)	R_{exp} (%)	R_b (%)
	Temp. (°C)	Time (h)	Atmosphere					
LNC_{T1}	750	18	Air	2.8627(1)	14.1562(9)	6.5	8.6	12.7
LNC_{T2}	800			2.8591(1)	14.160(1)	1.4	9.4	13.1
LNC_{T3}	850			2.85827(9)	14.1623(9)	3.6	7.2	12.1
LNC_{T4}	900			2.85882(9)	14.1579(5)	3.0	10.5	10.8
LNC_{T5}	950			2.8596(8)	14.1538(6)	3.5	9.1	11.1
LNC_{H1}	850	6		2.8601(1)	14.148(1)	1.9	7.2	12.8
LNC_{H2}		8		2.8583(1)	14.1460(9)	2.2	7.1	12.3
LNC_{H3}		12		2.85768(9)	14.1430(9)	0.6	7.1	12.9
LNC_{H4}		14		2.8575(1)	14.1432(9)	1.3	7.1	13.1
LNC_{H5}		18		2.85827(9)	14.1623(9)	3.6	7.2	12.1
LNC_{AO}	850	18	Oxygen	2.85832(9)	14.150(1)	1.2	9.1	11.3

Numbers in parentheses are statistical errors of the last significant digit. ϕ, Weight fraction of Li_2CO_3 phase. R_{exp} and R_b, refinement parameters. The subscripts: T, H and A stand for temperature, time and atmosphere, respectively

3 Results and discussion

3.1 Structure

Figure 1 shows XRD patterns of LNC_T sintered at 750–950 °C for 18 h in air. Figure 2 depicts X-ray diffractograms of LNC_H sintered at 850 °C for 6–18 h in air. Figure 3 represents XRD patterns of LNC_A sintered at 850 °C for 18 h in air and oxygen. The XRD patterns of LNC were similar to those reported earlier [10, 12]. The LNC exhibited an α-$NaFeO_2$-type hexagonal structure having a space group of $R\text{-}3m$ (166), lattice constants ($a = b$) of 2.8594(1) Å and c of 14.155(12) Å, cell volume (V) of 100.23 $Å^3$, theoretical density (ρ_{th}) of 4.85 g cm^{-3} and number of formula units in the unit cell (Z) of 3 [10, 12, JCPDS 87-1563]. An increase in sintering temperature and time improved the splitting and the relative intensity of hexagonal peaks relative to the main peak (2θ–19.7°). However, no significant difference in the XRD patterns of samples sintered in air and oxygen was observed. Some additional very weak reflection peaks, marked by an asterisk in the XRD patterns, also appeared most probably due to unreacted Li_2CO_3 [17]. Song et al. [20] considered these as superstructure peaks, resulting from super lattice ordering of atoms on the transitional metal layers.

As mentioned earlier, the synthesis condition largely influences the ordering on the 3a- and 3b-sites [3–6, 10–19]. Consequently, it affects the lattice constants (a and c) and the reflection peaks ratios, such as I_{003}/I_{104}, $(I_{006} + I_{102})/I_{101}$ and I_{108}/I_{110}. Therefore, lattice parameters of LNC are determined by the full profile Rietveld refinement method with the help of the Wyckoff atomic positions of $Li(Ni_{0.7}Co_3)O_2$ [10, 12]. The Li_2CO_3 phase was also included during Rietveld refinement for determining its lattice constants and weight fraction (ϕ). The Wyckoff atomic positions used for Li_2CO_3 were, Li (8f: 0.1968(4), 0.4454(7), 0.8334(6)), C (4e: 0, 0.0665(4), 0.25), O1 (4e: 0, 0.3213(4), 0.25) and O2 (8f: 0.1463(1), −0.0631(3), 0.3132(2)) [21]. The site occupancies of $Li(Ni_{0.7}Co_3)O_2$ were kept at fixed values consistent with the nominal stoichiometry, $Li/(0.7Ni + 0.3Co) = 1$, as suggested by the Rougier et al. [10] and Gover et al. [12]. An effect of impurity on the nominal stoichiometry of LNC was not considered due to very weak reflection peaks of impurity phase. It is also worth mentioning that the structural parameters of LNC, determined by Rietveld

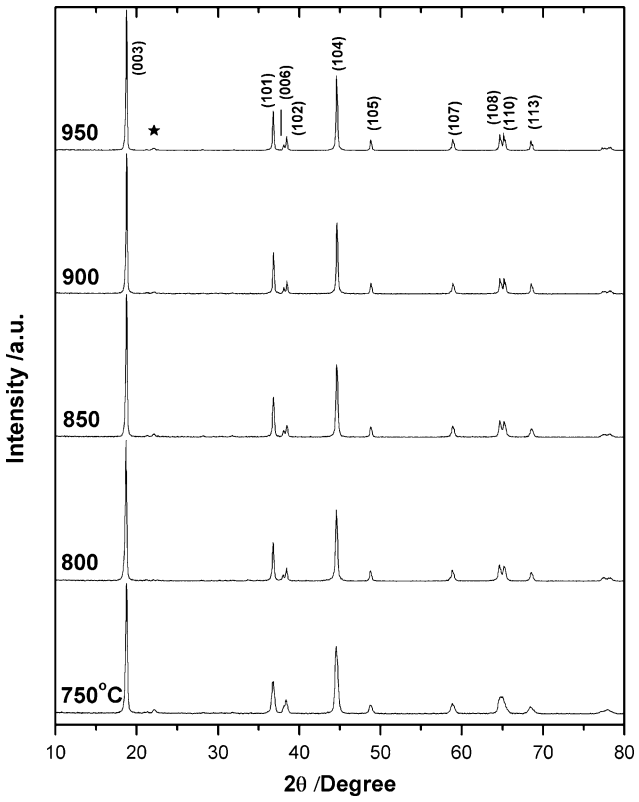

Fig. 1 XRD patterns of LNC_T sintered at different temperature for 18 h in air. Miller indices of the Bragg peaks are indicated near the each peak. *Asterisk*, Li_2CO_3 phase [JCPDS 72-1216]

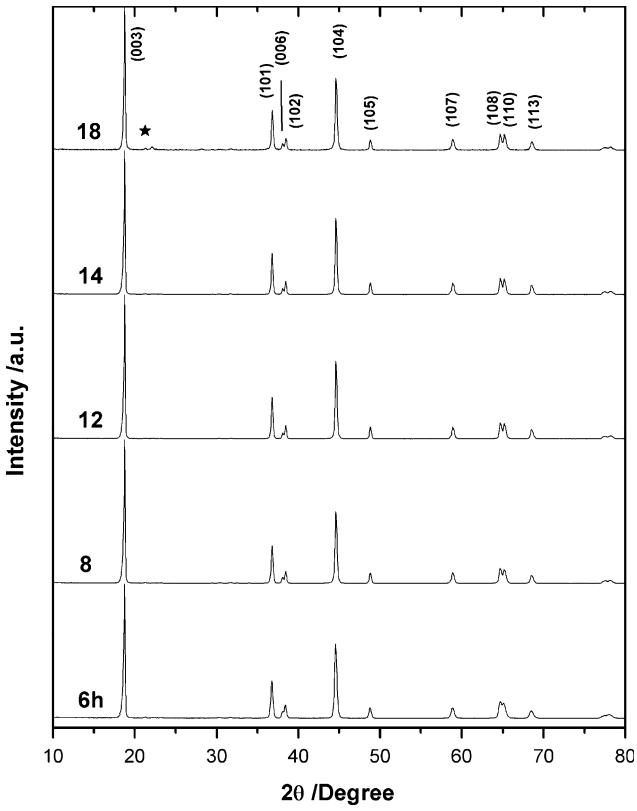

Fig. 2 XRD patterns of LNC_H sintered at 850 °C for different time in air. Miller indices of the Bragg peaks are indicated near the each peak. *Asterisk*, Li_2CO_3 phase [JCPDS 72-1216]

refinement and discussed below, were also found almost invariant with and without impurity. Figure 4 shows a typical Rietveld plot of LNC_{T1} containing the highest amount (~6 wt.%) of the impurity phase. The observed and calculated intensity profiles were well matched, which is obvious from the plot of their difference, as shown in the bottom of the figure. The refinement (*R*)-factors, shown in Table 1, were also close to each other for all the samples.

The lattice constants (*a* and *c*) of LNC prepared with different sintering conditions are presented in Table 1. Figure 5 shows unit cell volume and *c*/*a* ratio of LNC. The lattice constant, *a* corresponds to the interlayer metal–metal distance, while *c* equals to three times of sum of the interlayer spacing and the slab thickness. The following features were noted with increasing sintering temperature and time; (i) An increase in temperature decreased the

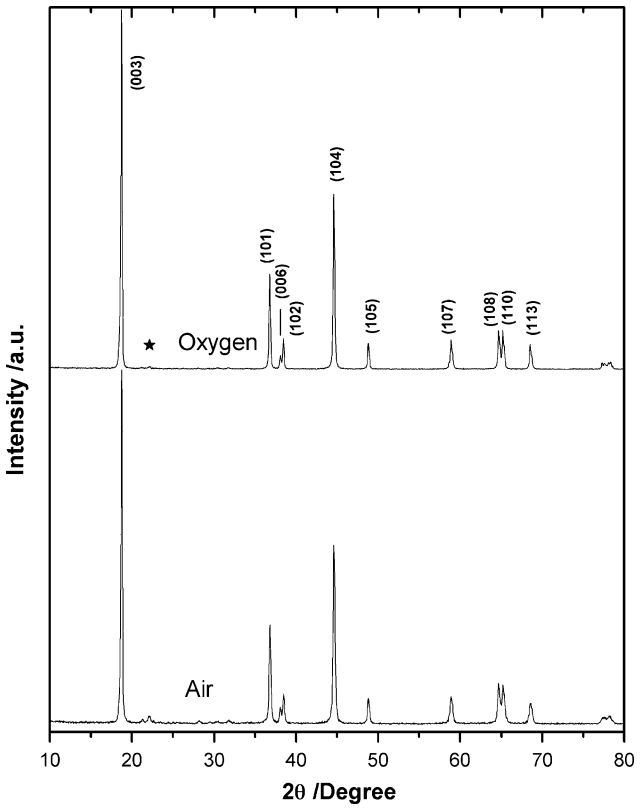

Fig. 3 XRD patterns of LNC_A sintered at 850 °C for 18 h in air and oxygen. Miller indices of the Bragg peaks are indicated near the each peak. *Asterisk*, Li_2CO_3 phase [JCPDS 72-1216]

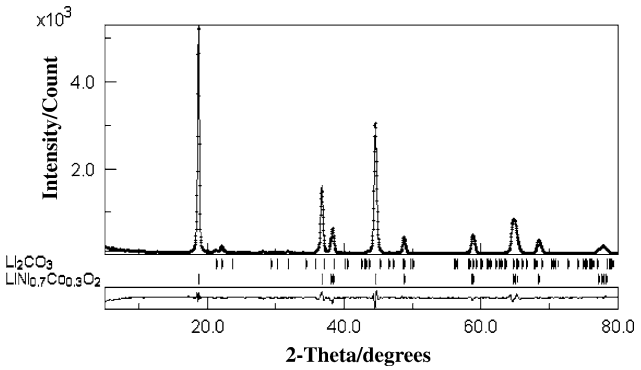

Fig. 4 Rietveld refined profile of the LNC_{T1} containing an impurity Li_2CO_3 phase. The solid line is calculated intensity and the plus is observed intensity (the background was not subtracted). The short vertical lines show the possible Bragg reflections. The bottom corresponds to the difference between observed and calculated intensities

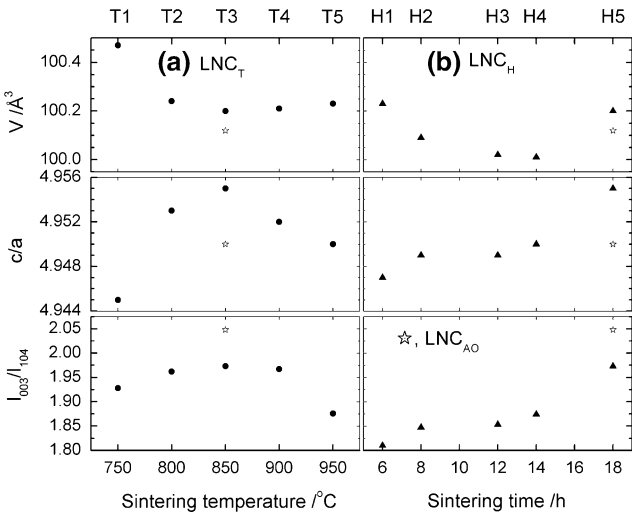

Fig. 5 Unit cell volume (*V*), *c*/*a* and I_{003}/I_{104} of **a** LNC_T sintered at different temperature for 18 h, and **b** LNC_H sintered at 850 °C for different time in air. *Asterisk*, LNC_{AO} sintered at 850 °C for 18 h in oxygen

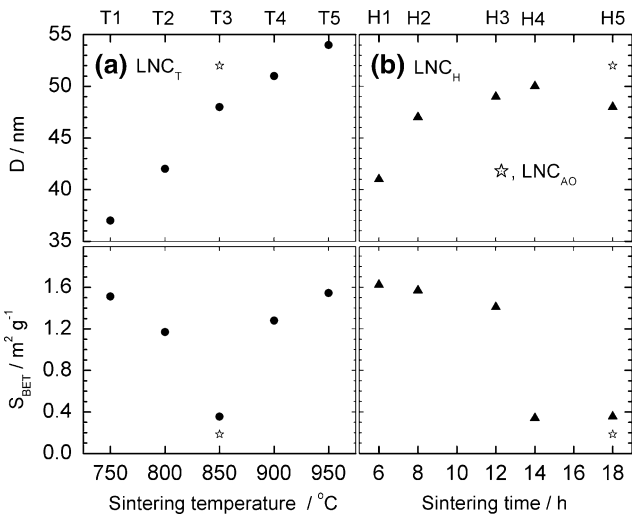

Fig. 6 Crystallite size (*D*) and BET surface area (S_{BET}) of **a** LNC_T sintered at different temperature for 18 h in air and **b** LNC_H sintered at 850 °C for different time in air. *Asterisk*, LNC_{AO} sintered at 850 °C for 18 h in oxygen

value of a and increased the value of c up to 850 °C. A reversal trend was noticed for the higher values of sintering temperature. This resulted in an optimal value for the cell volume and c/a ratio of LNC_{T3} sintered at 850 °C. (ii) The values of a and c decreased with sintering time up to ~14 h, and increased for 18 h. This led to the lowest cell volume for LNC_{H4} sintered for 14 h. This also resulted in slightly higher c/a ratio for LNC_{H4}, though it was less than the value of LNC_{H5} sintered for 18 h. Sintering in air and oxygen atmosphere also altered the value of c of the LNC. The value of c for LNC_{AO} sintered in oxygen was less than that for air sintered LNC_{H5} resulting in minima in cell volume and c/a ratio for LNC_{AO}. These findings are similar to those observed earlier for the $LiNi_{1-x}Co_xO_2$ with $x = 0.2$–0.25 mole [11, 13, 15–19].

A decrease in the lattice constant, a indicated an improvement in Li ordering on the 3a-site [3, 6, 11, 16, 17]. An increase in c inferred an improvement of Ni–Co ordering on the 3b-site probably due to proper rearrangement of Co^{3+} ions (radius = 0.53 Å) in NiO_2 layers (ionic radius of Ni^{3+} = 0.56 Å) [9–17]. A decrease in the unit cell volume and/or an increase in the c/a ratio for LNC_{T3}, LNC_{H4} and LNC_{AO} suggested an improvement in the hexagonal ordering (layered structure). Sintering at ≥900 °C and/or for 18 h in air resulted in a high value of unit cell volume and/or a low value of c/a ratio most probably due to a loss in 3a-site ordering by Li-volatilization [15–17, 19]. These results are substantiated by the reflection peaks ratio study, which has been discussed below.

Figure 5 shows I_{003}/I_{104} peaks ratio of LNC sintered at different conditions. The trends of I_{003}/I_{104} ratio with sintering temperature and time were similar to those observed for c/a ratio with temperature and time. The LNC_{T3} sintered at 850 °C for 18 h exhibited slightly high peaks ratio. The LNC_{H4} sintered for 14 h also exhibited relatively high peaks ratio; though it was less than that of LNC_{H5} sintered for 18 h. The LNC_{AO} sintered in oxygen exhibited a value of I_{003}/I_{104} ratio higher than that of the LNC_{H5} sintered in air. An increase in the I_{003}/I_{104} ratio suggests an increase in cation ordering on the 3b-site [13–15, 18]. Thus, LNC_{T3}, LNC_{H4} and LNC_{AO} possessed a better cation ordering. One can obtain similar information from the hexagonal reflection doublets, (006)/(102) and (108)/(110) for samples sintered at temperature higher than 800 °C in air or oxygen and with a sintering time greater than 12 h. The peak ratio $(I_{006} + I_{102})/I_{101}$, which is reciprocal to the hexagonal ordering, was 0.485 for LNC_{H5} and 0.473 for LNC_{AO} suggesting slightly improved hexagonal ordering for sample sintered in oxygen [13–15]. Also the LNC sintered at 850 °C for 14 h in air exhibited the lowest unit cell volume accompanied by relatively higher values of c/a ratio and I_{103}/I_{104} reflection peaks ratio.

As mentioned earlier, an impurity Li_2CO_3 phase was observed along with the primary LNC phase. The lattice parameters of Li_2CO_3 obtained after refinement were similar to those reported earlier [21]. A trace amount (<3.6%) of Li_2CO_3 was observed for the samples sintered higher than 750 °C (Table 1). This suggests that a pure $LiNi_{0.7}Co_{0.3}O_2$ phase can be obtained by using Li_2CO_3 precursor of ~1.05 mole instead of 1.08 mole as observed earlier by Hwang et al. [13].

3.2 Morphology

The particle size and particles distribution have a direct impact on the electrochemical properties of a cathode [3, 4, 11, 13–15]. The crystallite is a basic building block of powder morphology. It also indicates crystallinity of the powder. The crystallite size (D) of LNC is therefore calculated for the strongest peak and shown in Fig. 6. An increase in sintering temperature increased the value of D

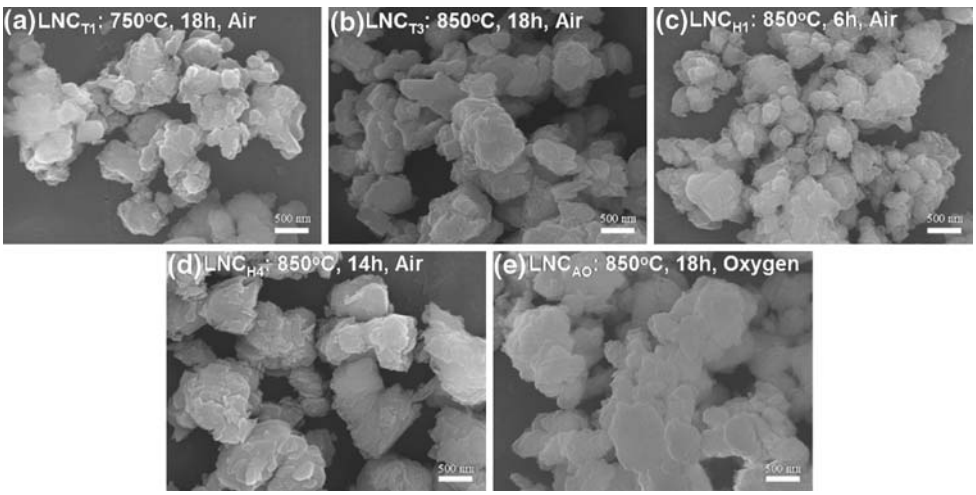

Fig. 7 SEM images of **a** LNC_{T1}, **b** LNC_{T3}, **c** LNC_{H1}, **d** LNC_{H4} and **e** LNC_{AO}, prepared by various sintering conditions. Bar, 100 nm at ×30,000 resolution

indicating an increase in crystallinity. An increase in sintering time also increased the D up to 14 h (LNC_{H4}), and then slightly decreased for 18 h inferring a better crystallinity for LNC_{H4}. The LNC_{AO} exhibited D-value relatively larger than that of LNC_{H5}. It is worth mentioning that the particle size (D_{BET}) and the BET surface area (S) are related by an expression, $S = 6/\rho_{th} \cdot D_{BET}$. Therefore, S is determined for understanding the effect of sintering condition on powder morphology of LNC and shown in Fig. 6. The value of S decreased up to 850 °C (LNC_{T3}) and then increased for higher sintering temperature. Similarly, S decreased with increasing sintering time up to 14 h (LNC_{H4}) and become almost invariant for 18 h. The value of S for LNC_{AO} was also low, relative to that of LNC_{H5}. A decrease in surface area or an increase in particle size with increasing sintering temperature/time is a common phenomenon; however, an increase in surface area for LNC_{T4} and LNC_{T5} is not clear. The powder morphology is also studied using scanning electron microscopy, and micrographs for LNC_{T1}, LNC_{T3}, LNC_{H1}, LNC_{H4} and LNC_{AO} are shown in Fig. 7. The primary particles were observed almost spherical for all the samples. An increase in sintering temperature and time increased the agglomeration, resulting in relatively large size of particles for the LNC_{T3} and LNC_{H4}. The agglomeration was relatively large for oxygen-sintered sample, LNC_{AO}. The average size of particles for LNC_{H4} was almost same and particles were distributed uniformly relative to LNC_{T3} and LNC_{AO}. Thus, superior morphological parameters i.e. low surface area and relatively large particle size were obtained for LNC_{T3}, LNC_{H4} and LNC_{AO} affecting the electrochemical properties of LNCs, as discussed below.

3.3 Electrochemical properties

The electrochemical properties of cells fabricated using LNC are examined by charge–discharge experiment at 0.1–2 C-rates. Figure 8 shows typical charge–discharge cycles carried out galvanostatically at 0.2 C for LNC_T sintered at (a) 750, (b) 850 and (c) 950 °C for 18 h in air. The electrochemical cycles were found similar to those observed earlier for the $LiNi_{1-x}Co_xO_2$ ($x = 0.2$–0.25 mole), prepared at various sintering temperature and time [13–19]. The discharge capacity of LNC_T, sintered at 750–950 °C for 18 h in air, as a function of (a) cycle number and (b) C-rate is shown in Fig. 9. Figures 10 and 11 show similar studies for LNC_H (sintered at 850 °C for 6–18 h in air) and LNC_A (sintered at 850 °C for 18 h in air or oxygen), respectively. One can note that an increase in sintering temperature up to 850 °C (LNC_{T3}) increased the discharge capacity with improved capacity retention. A further increase in sintering temperature decreased the discharge capacity. Similarly, an increase in sintering time

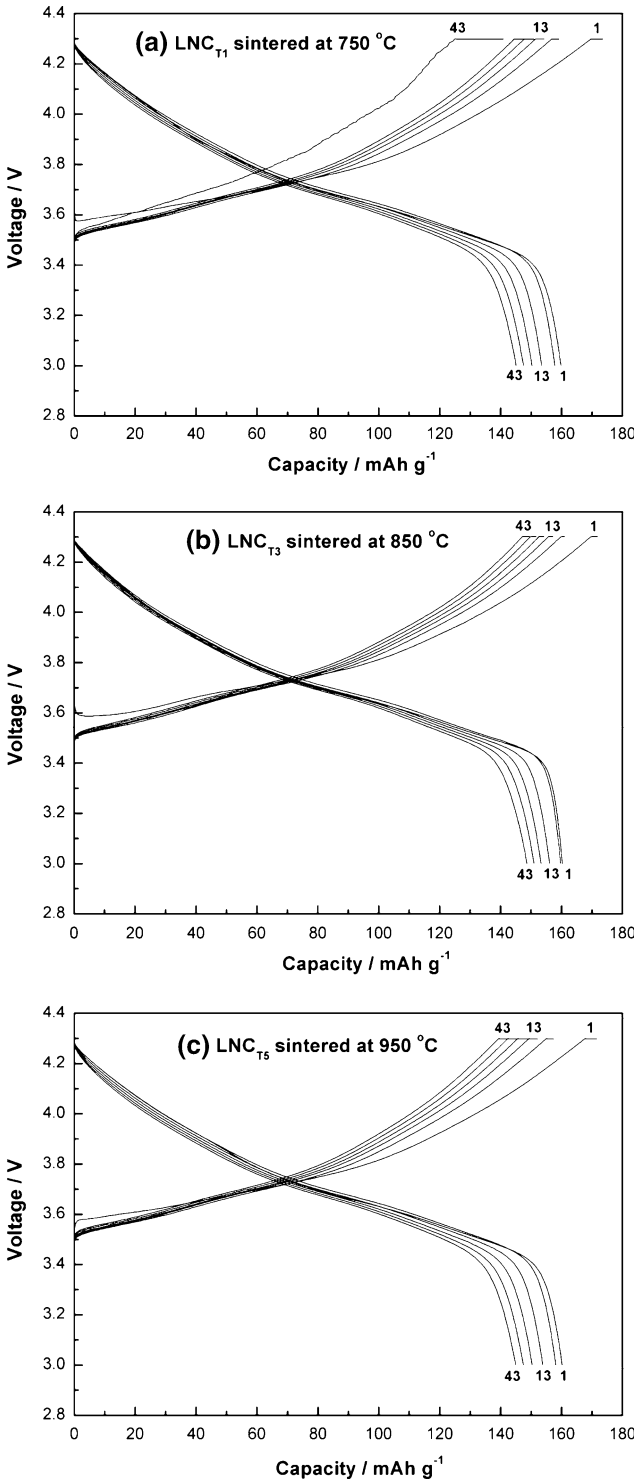

Fig. 8 Electrochemical charge–discharge cycles of **a** LNC_{T1}, **b** LNC_{T3} and **c** LNC_{T5} sintered at different temperatures for 18 h in air. C-rate, 0.2

up to 14 h (LNC_{H4}) improved the discharge capacity. An increase in sintering time to 18 h largely reduced discharge capacity. The capacity retention was the highest for

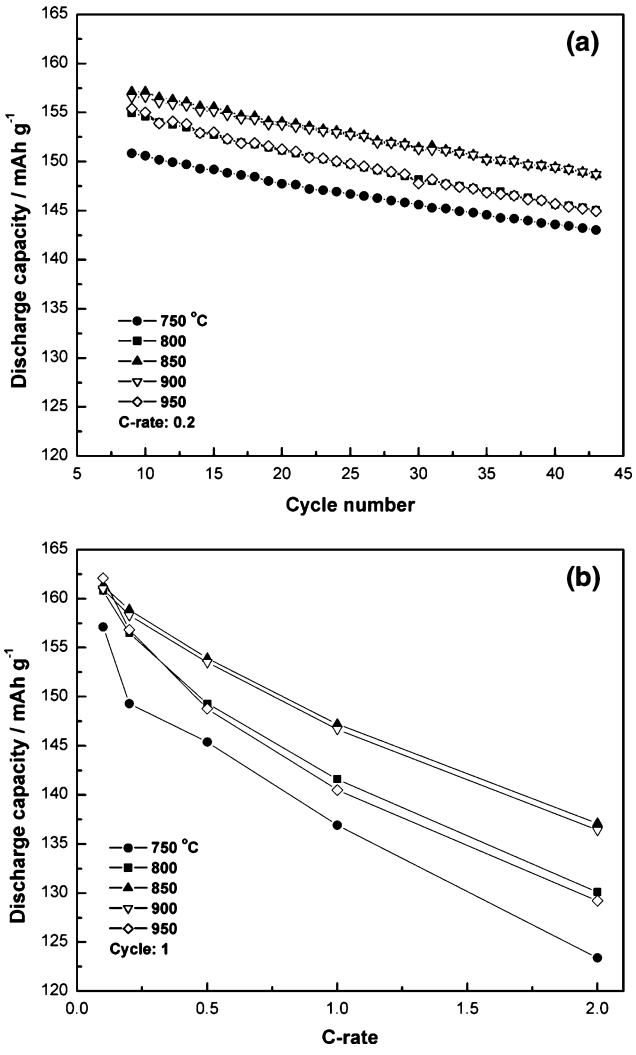

Fig. 9 Discharge capacity versus **a** cycle number and **b** C-rate of LNC_T sintered at different temperature for 18 h in air

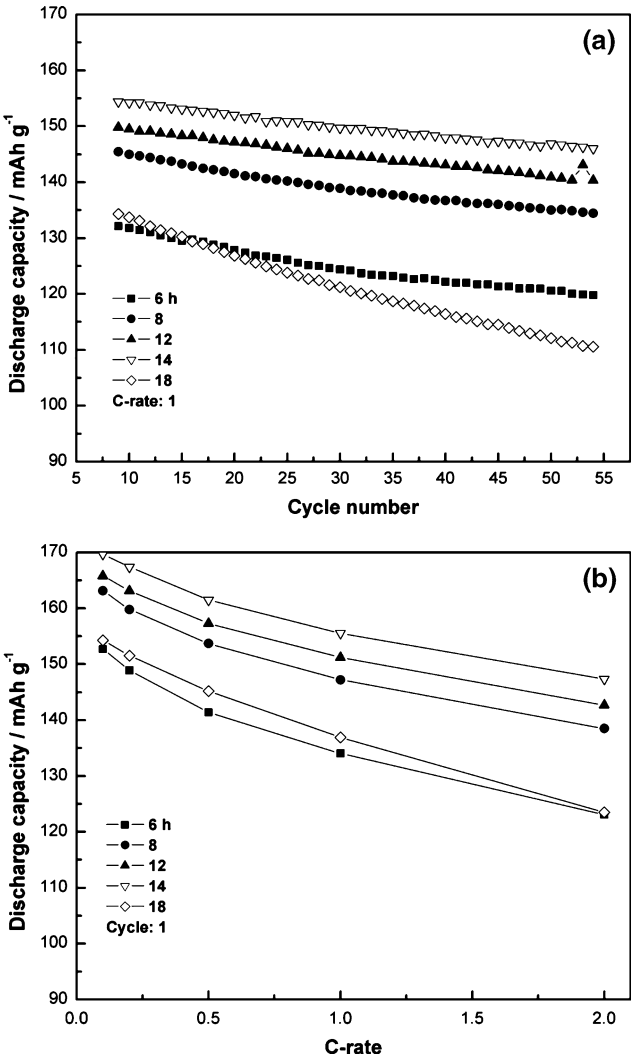

Fig. 10 Discharge capacity versus **a** cycle number and **b** C-rate of LNC_H sintered at 850 °C for different time in air

LNC_{H4}. Sintering in oxygen helped, though a little, to improve the discharge capacity. Figures 9b–11b also showed a decrease in discharge capacity with increasing C-rate.

The electrochemical cell parameters for the 1st and 43rd cycles, such as charge–discharge capacity and Coulombic efficiency along with the irreversible capacity loss of LNC are shown in Table 2. The charge–discharge capacity and Coulombic efficiency were noticed relatively higher for LNC_{T3}, LNC_{H4} and LNC_{AO}. The irreversible capacity loss was also relatively lower for LNC_{T3}, LNC_{H4} and LNC_{AO}. These samples exhibited a low value of unit cell volume accompanied with comparatively higher values of c/a and I_{003}/I_{104} ratios, which suggested an improved hexagonal ordering. A relatively lower BET surface area and relatively higher particle/crystallite size for these samples also helped to decrease the interfacial contact between cathode and electrolyte, which is a major factor of the capacity fade via decomposition of electrolytes and the dissolution of cathode active material [11, 13, 14]. The electrochemical study also indicated that a large crystallite/particle size observed for sintering temperature greater than 850 °C and/or sintering time greater than 14 h is unfavorable due to poorer kinetics. These studies establish a relation between the structure, the crystallinity, the morphology and the electrochemical properties observed earlier for the $Li(Ni_{1-x}Co_x)O_2$ with $x = 0.2$–0.25 mole [10–19].

The highest charge–discharge capacity and Coulombic efficiency, and the smallest irreversible capacity loss were observed for LNC_{H4} sintered at 850 °C for 14 h in air. This could be attributed to the lowest unit cell volume, higher

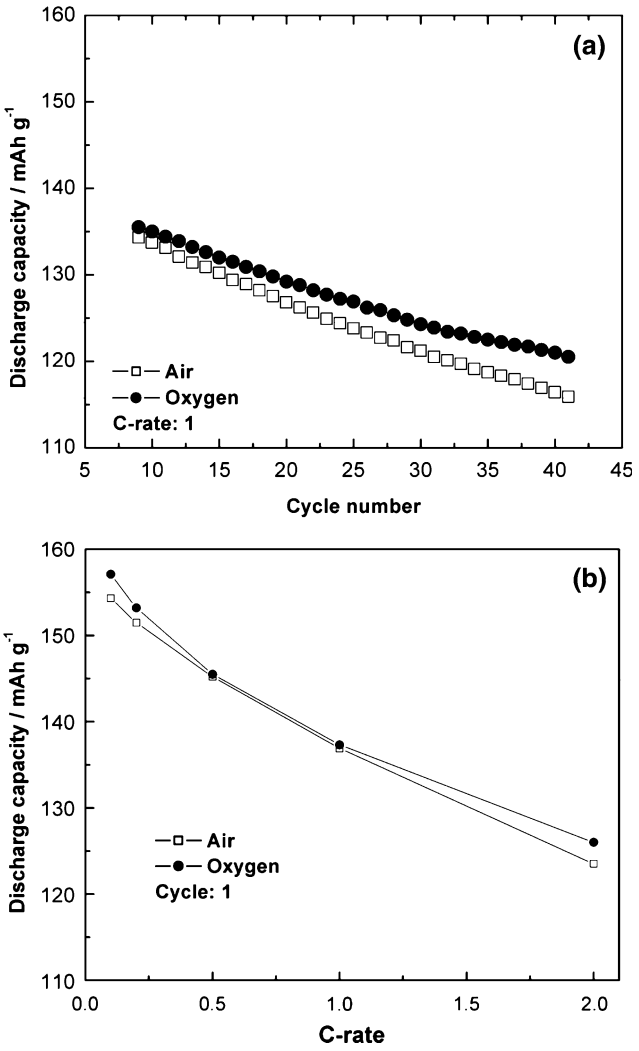

Fig. 11 Discharge capacity versus **a** cycle number and **b** C-rate of LNC_A sintered at 850 °C for 18 h in air (LNC_{H5}) and oxygen (LNC_{AO})

c/a and I_{003}/I_{104} ratios, the lowest BET surface area and higher crystallite/particle size along with a uniform particle size distribution. LNC_{H4} exhibited electrochemical properties better than those observed for $LiNi_{0.8}Co_{0.2}O_2$ sintered at 800 °C for 24 h [18]. The $LiNi_{0.8}Co_{0.2}O_2$ exhibited discharge capacity of 161 mAh g^{-1} for 1st cycle and 155 mAh g^{-1} for 10th cycle at a 0.1 C. The electrochemical parameters of LNC_{H4} were also better than those reported earlier by Gover et al. for LNC [12]. They reported 1st charge capacity of 184 mAh g^{-1}, 1st discharge capacity of ~156 mAh g^{-1}, 15th charge capacity of 137 mAh g^{-1} and 15th discharge capacity of 137 mAh g^{-1}. Their overall discharge efficiency was also low (~88%) as compared to that of LNC_{H4} (~95%). The superior electrochemical properties of LNC_{H4} are may be due to the optimal sintering conditions that help to improve the hexagonal ordering, crystallinity and the morphology [11–19].

4 Conclusions

A cathode active material, $Li(Ni_{0.7}Co_{0.3})O_2$ was synthesized by the co-precipitation method. Sintering conditions, namely temperature, time and atmosphere, were varied for optimizing the electrochemical cell parameters. The electrochemical properties were explained using the structure, crystallinity and morphology studies. Samples sintered at 850 °C for 14 h in air exhibited the superior electrochemical properties most probably due to improved hexagonal ordering, crystallinity and morphology. It was found that it exhibited electrochemical properties better than those reported for $Li(Ni_{1-x}Co_x)O_2$ ($x = 0.2$–0.3 mole).

Table 2 Electrochemical cell parameters of LNC synthesized at different sintering conditions

Sample	1st Cycle			43rd Cycle			Capacity loss (%)
	Charge capacity (mAh g^{-1})	Discharge capacity (mAh g^{-1})	Coulombic efficiency (%)	Charge capacity (mAh g^{-1})	Discharge capacity (mAh g^{-1})	Coulombic efficiency (%)	
LNC_{T1}	173.7	159.8	92.0	145.7	145.1	99.6	9.2
LNC_{T2}	165.7	154.6	93.3	141.3	143	101.2	7.5
LNC_{T3}	172.0	160.2	93.1	149.6	148.7	99.4	7.2
LNC_{T4}	172.3	159.6	92.6	149.7	148.7	99.3	6.8
LNC_{T5}	171.7	160.2	93.3	143.5	144.3	100.6	9.9
LNC_{H1}	168.4	133.9	79.5	125.0	122.0	97.6	8.9
LNC_{H2}	179.6	147.4	82.1	140.6	136.7	97.2	7.3
LNC_{H3}	180.6	150.8	83.5	145.8	142.8	97.9	5.3
LNC_{H4}	182.5	155.1	85.0	151.1	147.9	97.9	4.6
LNC_{H5}	161.6	136.0	84.2	119.5	115.9	97.0	14.8
LNC_{AO}	181.7	135.0	74.3	124.5	120.5	96.8	10.7

The subscripts: T, H and A stand for temperature, time and atmosphere, respectively

References

1. Hassoun J, Reale P, Scrosati B (2007) J Mater Chem 17:3668
2. Horiba T, Maeshima T, Mataumura T, Koseki M, Arai J, Muranaka Y (2005) J Power Sources 146:107
3. Fu LJ, Liu H, Li C, Wu YP, Rahm E, Holze R, Wu HQ (2005) Prog Mater Sci 50:881
4. Wu YP, Rahm E, Holze R (2002) Electrochim Acta 47:3491
5. Wakihara M (2001) Mater Sci Eng R 33:109
6. Liu H, Wu YP, Rahm E, Holze R, Wu HQ (2004) J Solid State Electrochem 8:450
7. Sun Y, Wan P, Pan J, Xu C, Liu X (2006) Solid State Ionics 177:1173
8. Arai H, Okada S, Sakurai Y, Yamaki YI (1998) Solid State Ionics 109:295
9. Aria H, Okada S, Ohtsuka H, Ichimura M, Yamaki J (1995) Solid State Ionics 80:261
10. Rougier A, Saadoune I, Gravereau P, Willmann P, Delmas C (1996) Solid State Ionics 90:83
11. Gover RKB, Yonemura M, Hirano A, Kanno R, Kawamoto Y, Murphy C, Mitchell BJ, Richardson JW Jr (1999) J Power Sources 81–82:535
12. Gover RKB, Kanno R, Mitchell BJ, Hirano A, Kawamoto Y (2001) J Power Sources 97–98:316
13. Hwang BJ, Santhanam R, Chen CH (2003) J Power Sources 114:244
14. Gong ZL, Liu HS, Guo XJ, Zhang ZR, Yang Y (2004) J Power Sources 136:139
15. Periasamy P, Kim HS, Na SH, Moon SI, Lee JC (2004) J Power Sources 132:213
16. Gover RKB, Kanno R, Mitchell BJ, Yonemura M, Kawamoto Y (2000) J Electrochem Soc 147:4045
17. Gover RKB, Kanno R, Mitchell BJ, Hirano A, Kawamoto Y (2000) J Power Sources 90:82
18. Fey GTK, Shiu RF, Subramanian V, Chen JG, Chen CL (2002) J Power Sources 103:265
19. Liu H, Li J, Zhang Z, Gong Z, Yang Y (2003) J Solid State Electrochem 7:456
20. Song CH, Stephan AM, Jeong SK, Hwang YJ, Kim AR, Nahm KS (2006) J Electrochem Soc 153:A390
21. Idemoto Y, Richardson JW Jr, Koura N, Kohara S, Loong CK (1998) J Phys Chem Solids 59:363